

# The First U.S. Naval Observatory Robotic Astrometric Telescope Catalog (URAT1)

N. Zacharias<sup>1</sup>, C. Finch<sup>1</sup>, J. Subasavage<sup>2</sup>,  
 G. Bredthauer<sup>3</sup>, C. Crockett<sup>2</sup>, M. Divittorio<sup>2</sup>, E. Ferguson<sup>1</sup>, F. Harris<sup>2</sup>, H. Harris<sup>2</sup>,  
 A. Henden<sup>4</sup>, C. Kilian<sup>1</sup>, J. Munn<sup>2</sup>, T. Rafferty<sup>5</sup>, A. Rhodes<sup>2</sup>, M. Schultheiss<sup>2</sup>, T. Tilleman<sup>2</sup>,  
 and  
 G. Wieder<sup>1</sup>  
 nz@usno.navy.mil

## ABSTRACT

URAT1 is an observational, astrometric catalog covering most of the  $\delta \geq -15^\circ$  area and a magnitude range of about  $R = 3$  to 18.5. Accurate positions (typically 10 to 30 mas standard error) are given for over 228 million objects at a mean epoch around 2013.5. For the over 188 million objects matched with the 2MASS point source catalog proper motions (typically 5 to 7 mas/yr std. errors) are provided. These data are supplemented by 2MASS and APASS photometry. Observations, reductions and catalog construction are described together with results from external data verifications. The catalog data are served by CDS, Starsbourg (I/329).

*Subject headings:* astrometry, proper motions, catalogs

## 1. Introduction

The U.S. Naval Observatory (USNO) Robotic Astrometric Telescope (URAT) project was conceived as next step beyond the successful USNO CCD Astrograph Catalog (UCAC) project (Zacharias et al. 2013) providing accurate reference star positions on the sky at current epochs before Gaia<sup>1</sup> data become available. Original plans called for a new, dedicated 1-meter class telescope ((Zacharias 2002), (Zacharias 2004), (Laux & Zacharias 2005), (Zacharias et al. 2006)). Primarily due to its cost, the instrument was not built. However, the detector development initiated by a Small Business Innovation Research (SBIR) through the Office of Naval Research lead

to the manufacturing of the world’s largest, monolithic detector, the STA1600. In 2008 funding became available for a large focal plane instrument consisting of 4 of those 111 million pixel detectors. The USNO “redlens” astrograph (1) previously used for the UCAC survey (Zacharias et al. 2013) was completely rebuilt by the USNO instrument shop in Washington DC. A single truss-tube structure now joins the old lens and the new focal plane dewar, utilizing the 9 degree diameter field of view.

After initial tests in September 2011 in Washington DC, the telescope was deployed to the Naval Observatory Flagstaff Station (NOFS) in Arizona in October 2011. Upgrades to the dome for lightning protection were installed, subsequent hardware issues resolved, and operational robustness improved. Survey operations began in April 2012.

A wide dynamic range of stars between about  $R = 3$  and 18.5 mag are being observed with a combination of long exposures and short exposures with an objective grating. With multiple sky overlaps per year and its high precision URAT is aiming at

<sup>1</sup>U.S. Naval Observatory, Washington DC

<sup>2</sup>Naval Observatory Flagstaff Station, AZ

<sup>3</sup>Semiconductor Technology Associates, San Juan Capistrano, CA

<sup>4</sup>AAVSO, 49 Bay State Rd., Cambridge, MA 02138

<sup>5</sup>USNO, retired

<sup>1</sup>sci.esa.int/gaia, www.cosmos.esa.int/web/gaia

2 specific goals: first, to establish a highly accurate, dense, deep optical reference frame at current epochs; and second, to identify nearby stars without selection effects by directly observing trigonometric parallaxes in an all-sky survey.

Unfortunately the project was delayed due to various technical and funding issues and is now running close to Gaia data releases. However, accurate reference stars in the northern hemisphere (URAT1) are available now, over a year prior to an anticipated first Gaia data release. Northern hemisphere observing was completed in June 2015 and the instrument is being packed up for deployment to the Southern Hemisphere. More information about this project and potentially upcoming data releases is available at our web page [www.usno.navy.mil/USNO/astrometry/optical-IR-prod/urat1](http://www.usno.navy.mil/USNO/astrometry/optical-IR-prod/urat1).

The main purpose of URAT1 is to provide the astronomical community with a reference star catalog for current epochs about 4 times more precise than UCAC with a density similar to the Two-Micron All Sky Survey (2MASS) (Skrutskie et al. 2006), which is on average a factor of 4 improvement over UCAC4. Science drivers for accurate positions include: assist in predictions of solar system bodies occultations, improve accuracy of positions of moving objects referenced to the sky background (inertial reference star catalog), and link of the radio and optical coordinate systems.

Although URAT1 proper motions are very useful for stars fainter than the UCAC limit, they are only preliminary. Particularly for stars in the 8 to 14 mag range UCAC4 has better proper motions than URAT1 with corresponding more precise positions at much earlier epochs than 2014.

URAT1 is neither complete (maybe on 90% level) nor free of contamination (expected to be less than 0.5%). Systematic errors in positions are estimated to be on the 10 mas level, while systematic errors in proper motions are on the 1 to 2 mas/yr level.

The URAT1 catalog is presented as a collection of binary data files (total about 18 GB) with index file, auxiliary software and info. These data are served by CDS, Strasbourg. There is no data release on DVD. This paper accompanies the URAT1 catalog release and provides the scientific

rationale, reduction details, and results. User of URAT1 are also referred to the “readme” file included with the data release.

## 2. Observations

### 2.1. Instrument

Basic information about the telescope and camera is provided in Table 1. All observations utilize the same 5-element “redlens” which also was used for the UCAC program. A single, fixed bandpass (680 to 762 nm) is provided by the dewar window which serves as filter. The bandpass for URAT was pushed as far red as possible to reduce effects of atmospheric turbulence on the astrometry.

Focusing is performed by moving the lens because the back end dewar is much heavier than the lens. The dewar hold time is just over 24 hours, during which time about 25 kg of  $LN_2$  are boiled off. To compensate for this change in weight, a counterweight is moved along an arm on the opposite side of the pier to keep the telescope balanced.

A custom made shutter from Bonn University (Klaus Reif) is used. The layout of the focal plane is shown in Fig. 1. The gap between the main CCDs (labeled A to D) is 1200 arcsec. Each of the 4 main CCDs covers a sky area of  $2.65^\circ$  by  $2.65^\circ = 7$  square degrees.

For part of the observing program (see below) a diffraction grating is mounted in front of the lens. First order diffraction images saturate for stars about 5.0 mag brighter than for the central images, thus expanding the dynamic range of the survey enormously. The STA1600 CCDs also feature clocked anti-blooming (CAB) which drains electrons near saturation to avoid bleeding of charge into neighboring pixels. This allows to obtain accurate centroid fits of stars about 1.5 to 2.5 magnitudes brighter than traditional saturation, thus further extending the dynamic range of URAT data toward bright stars. Fig. 2 shows the brightness range of stars covered by various exposure times and modes of operation.

The STA1600 CCDs are back-side illuminated with optimized quantum efficiency near the URAT bandpass. The CCDs have few to none column defects. The CCDs are operated at normally  $-100^\circ\text{C}$ . Each main CCD has 8 readout ports going to one side of the CCD. All 4 CCDs are read

in parallel in about 20 seconds with a read noise of about  $10 e^-$  RMS. Full well capacity is at about  $80 ke^-$  and the gain is set to fully utilize the available dynamic range with 16 bit output.

A fiberglass dome with added metal mesh and other lightning protection measures is used. To improve the dome seeing, air is sucked out from the floor near the telescope mount which provides a steady air flow down through the dome slit while observing.

## 2.2. Survey fields and exposures

A basic pattern of survey fields was adopted with the same gap size between adjacent telescope pointings CCD footprints as the gap size between the 4 CCDs in the focal plane. To fill in the gaps, 2 more of the basic pattern of fields were overlaid with diagonal offsets. For each of these 3-times basic pattern of fields, a 5-fold dither pattern was adopted leading to a total of 15-fold overlap of fields. Due to the gaps this results in an average of 12 fields covering every area on the sky.

A 60 sec and a 240 sec exposure are taken on each such survey field. To cover a wide parallax factor range, the night is split into 5 parts of equal duration. Utilizing 1 dither position per part of the night, the corresponding 3-times basic pattern of fields is observed during each part of the night. Thus the entire pattern of 15 overlap of fields is observed once per year. Priority is given to high-declination fields. The southern limit of the survey is then determined by the available hours of observing which varies by season.

The above mentioned regular survey operation is run for about 3 weeks in a month without an objective grating. During the week around full Moon, the same pattern is observed again with short exposures (mostly 10 and 30 sec, sometimes 20 and 30 sec) and with an objective grating mounted in front of the lens.

Fig. 3 shows the mean number of observations per star (around magnitude 14, i.e. best case with data from almost any exposure) as found in the URAT1 catalog. More color plots, like mean number of URAT1 stars per square degree are provided with the data release in the “info” folder. URAT1 covers almost all northern sky and most of the area  $\delta \geq -15^\circ$ , plus the far south area around Pluto.

## 2.3. Robotic operations

The entire operations is controlled by a single Linux computer. The top level URAT operations control software and reduction code is written in Fortran. C-code routines are called for hardware interfaces to 3 systems: telescope, main CCDs, guide CCDs. Most telescope functions are routed through a Galil controller. HomeDome provided an interface to control dome shutter and dome rotation.

Every afternoon an “observer” needs to come to the telescope to unhook the  $LN_2$  line, verify safety of operations, and check on system status. A single command initiates auto-mode operations. The observer then notes the time of the  $LN_2$  fill and paths to save/backup the night’s data. The counter weight position is then automatically calculated and moves to position. The system is then in a loop mode checking weather conditions and time. The dome automatically opens around sunset and blowers turn on to equalize the temperature in the dome. A focus sequence is run and evaluated during twilight and survey observations begin when skies are sufficiently dark. System e-mails are sent for dome open/close and emergency notifications. Observing progress can be monitored remotely with a command line interface.

The control software has a wait loop before each observation where weather and safety conditions are monitored. A Boltwood cloud sensor unit is used for checking weather conditions and UPS units are monitored for power outages. In case of bad weather, the software will close the dome and wait for the conditions to improve. In case of power failure, UPS batteries are sufficient for the software to close the dome and power off the computers. A watch script is used to monitor the control code. If the software hangs up, the watch script will initiate a shutdown sequence, closing the dome and parking the telescope. The HomeDome system itself will shut down the dome if it loses communication with the control computer.

A triple fail-safe system is used to prevent the telescope from hitting something. Software limits are set for safe operations. In case they fail, optical limit switches stop the telescope motion. In case of a complete telescope control failure, mercury limit switches directly cut power to the telescope motion in case it exceeds limits in telescope

pointing with respect to the horizon.

At the end of the night the pixel data and log files are ftp'ed to a second Linux computer and reductions and backups are initiated automatically, which sometimes run into early next night. The "observer" or instrument shop personnel connects the  $LN_2$  line sometime in the morning before the auto-fill begins. The only other human interaction is for putting the grating on/off once a month, checking on desiccant cartridge at the lens, changing hard disk drives about once every week or two, and troubleshooting. The project encountered a fair amount of down time early on due to dome upgrades for lightning protection and associated side effects. Recent operations are very stable with only occasional need for a re-boot of the control computer and/or Galil interface and implementing control software fixes after mandatory operating system kernel updates.

#### 2.4. Guiding and focus control

All exposures of 30 sec duration or longer are guided. The 3 smaller CCDs mounted at the edge of the field of view are used to take about 4 sec long exposures. These images are read out and evaluated in real time. Mean telescope pointing corrections are thus derived every about 6 sec and fed to the mount before the next cycle of guide exposures begins.

The 3 guide CCDs are mounted at different distances with respect to the focal plane: intra-focal, in focus, extra-focal. At the end of a guided exposure the mean observed image profile width of each guide CCD is used to adjust the focus if needed. The complex lens is sensitive to temperature and temperature history, so frequent (about 20) focus changes are performed throughout the night.

#### 2.5. Quality control

After the automatic pixel processing is completed, a project scientist generates and looks at 5 pages of quality control plots of the data of the previous night. Occasionally manual reductions are run in steps in case of a failure of a system. Flags indicating possible problems are raised automatically and the project scientist has access to various, detailed log files for troubleshooting if needed.

Limits are set on mean image elongation, im-

age profile width, saturation and limiting magnitude for an exposure to meet survey quality. Mean number of detected objects per readout tab are compared to identify potential missing data. Rejected exposures are noted and picked up automatically by the scheduling software for next night observations. The quality control pipeline was not fully available until end of 2012 and early survey data were only spot-checked with few fields re-observed.

#### 2.6. Darks, flats, photometry

Darks for all standard exposure times are taken several times per year. A few sets of sky flats were obtained throughout the project, taken near sunset with a piece of white cloth covering the lens. The pixel-to-pixel sensitivity variations are found to be small and stable. Emphasis of this program is on astrometry and only minimal effort was put into providing URAT bandpass photometry. Survey quality observations often were obtained during partly cloudy nights or with cirrus present. No dedicated observations of photometric standard stars were performed, and all observations are taken within about  $5^\circ$  (20 min) of the meridian.

#### 2.7. Astrometric calibration observations

For normal operations the astrograph is on the east side of the pier. A few times throughout the project, the telescope is flipped to the west side of the pier allowing observations with the focal plane rotated by  $180^\circ$  with respect to the sky. The same field is observed on the same CCD in both orientations allowing to detect and calibrate possible magnitude dependent systematic errors of star positions caused by the instrument alone. In another calibration observing run the same fields are being observed with the objective grating on and using short (typically 30 sec) and long (240 sec) exposures. Mapping of  $x, y$  centroid positions of stars observed with such pairs of exposures allows to compare positions of the same stars as observed with 1st order grating images and central images, as well as comparing data of saturated and not saturated images of the same stars.

## 2.8. Data used for URAT1

For the URAT1 catalog reduction 57,129 exposures (of a total of 65,639) from 2012 April 24 until 2014 June 21 were selected, meeting acceptable quality standards. A total of 14 and 12 exposures of the Pluto field area taken 2013 Sept 19 and 2014 Sept 06, respectively, were added. These fields were observed to support occultation predictions. Altogether data from 380 nights were used for URAT1. This includes some special observing like bright stars and astrometric calibration exposures (see above). The distribution of observations by month are shown in Fig. 4. Clearly a seasonal pattern is seen with fewer exposures than average taken in winter and summer (monsoon). Grating survey observing became routine about half a year into the program.

A small fraction of data was dropped during the reduction process. In particular, if too few reference stars were matched or conventional astrometric solutions were poor, those exposures were just not included in upstream processing. Similarly all individual “problem stars” like blended images were dropped.

The URAT data for this first release was split into 38 sets, 19 each for grating and regular survey data. All grating observations taken within about a week around each full Moon were collected into a set. All data taken between 2 such grating observing runs comprise a set of regular survey data. In few cases with sparse data, a set extends over about 7 weeks.

## 3. Reductions

The camera output is written to 2-byte unsigned integers in FITS format with very basic header data, while observing log files are kept as separate text files. All raw image processing, photometric and astrometric reductions were performed with custom Fortran code, building on the software used for the UCAC program. IRAF and DS9 were used to display sample data and perform image examinations for spot checks, algorithm development and trouble shooting. Each of the 4 main camera CCDs was handled separately throughout the reductions, as if data were taken with a different telescope for each CCD.

## 3.1. Pixel data and centroids

Raw CCD exposures were bias corrected from overscan data. A mean dark of corresponding exposure time and epoch was subtracted and a mean flat applied. No extra bias frames were utilized.

Background level and noise were calculated from histogram data of sub-areas. Objects were detected with a threshold of 4-sigma above the background. Basic image profile properties like elongation and start parameters for the center fit were obtained from moment analysis of the pixels forming that image. Object centers were determined from a least-squares fit of the pixel data using a 2-dimensional circular symmetric Gaussian image profile model function. Only objects with a successful fit were propagated to the next step in the reduction process.

Fig. 5 shows sample results for an exposure taken with the grating. The CAB feature of the CCD enables a dynamic range of almost 10 magnitudes. Saturation is at about 30 kADU or instrumental magnitude 6.5. First order diffraction images have an average elongation of about 1.1 (ratio of major to minor axis of image), and a significantly larger fit radius than the central images. The image center fit precision is below 10 milli-pixel over several magnitudes, including the CAB regime up to 2.5 magnitudes brighter than the traditional saturation limit.

## 3.2. Photometry

Instrumental magnitudes were derived from the volume of the 2-dim Gaussian image profile fits, not from aperture photometry. These magnitudes were calibrated with APASS R and R-I data in a linear fit to derive a zero-point constant between the instrumental and calibrated URAT bandpass magnitudes. An example is given in Fig. 6 for a single exposure and CCD. The formal error of a zero-point constant is typically around 0.01 mag. Many URAT observations were performed in non-photometric conditions and URAT photometry is believed to be accurate on a few percent level at best. Errors on URAT1 magnitudes as given in the catalog are derived from scatter of individual observations with 0.01 mag error floor RMS added.

### 3.3. Grating image merge

For all grating exposures, individual images in the  $x, y$  data files were identified as belonging to a central or first order or higher order diffraction image by taking into account the brightness, location and elongation information. The algorithm to identify these images was refined by looking at pixel data with the IRAF “tvmark” feature to highlight various types of images. An arithmetic mean position was calculated from a matching pair of first order grating images. In addition, all central images were kept as separate observation. Thus some stars have 2 observations per exposure based on central image and first order diffraction images, respectively. All single first order images and all higher order images are rejected.

### 3.4. Astrometric solution

A subset of the UCAC4 (Zacharias et al. 2013) stars, those with astrometry flag “good” and in the magnitude range of 8.0 to 16.0, were used as reference stars in a conventional, weighted least-squares adjustment of URAT data to obtain  $\alpha, \delta$  positions. Using our custom software, reference stars were matched with the  $x, y$  data utilizing telescope pointing data from the observing log files.

Due to the large field of view, an 8-parameter plate model was adopted which includes 2 tilt terms ( $p, q$ ) besides the full linear model ( $a$  to  $f$ , split into orthogonal and non-orthogonal terms):

$$\begin{aligned}\xi &= ax + by + c + ex + fy + px^2 + qxy \\ \eta &= -bx + ay + d + fx - ey + qy^2 + pxy\end{aligned}$$

Here  $\xi, \eta$  are the standard coordinates (scaled from radian to arcsec) and  $x, y$  the observed center coordinates of star images on the CCD (scaled from pixel unit to arcsec). This approach is feasible due to the large number of reference stars available per CCD ranging from a few hundred to several thousand.

The root-square-sum formal errors of UCAC4 reference star positions at URAT observing epochs, the formal errors of URAT  $x, y$  data and an atmospheric turbulence contribution (20 mas for 100 sec exposure, scaled by square root of exposure time) were used as weights in the astrometric

solution. For most stars the largest error contribution is from the UCAC4 proper motion errors. Fit results after excluding over 3-sigma outliers show on average only about 10% larger values than expected from the combination of all known, estimated error contributions, which easily could have been underestimated by that amount.

Astrometric solution errors are independent of the number of reference stars available for individual exposures. There is a significant variation of the astrometric solution error as a function of Declination, which can be explained by the mean epoch differences between URAT1 and UCAC4 data. The area near the celestial north pole was observed last in the UCAC4 program leading to the smallest epoch differences to URAT1 data, thus to the smallest UCAC4 position errors at URAT1 epoch due to error propagation of the UCAC4 proper motion errors.

The CCDs were found to be aligned to  $\alpha, \delta$  to within 13 and 36 arcmin, with  $x$  being along  $\delta$ . The plate tilt parameters were found to be significant and vary as expected by zenith distance (telescope tube bending and other effects, like alignment of lens with respect to focal plane after focus changes).

Fig. 7 shows an example of reference star residuals as a function of magnitude. Data from an entire set of grating observations over 5 nights in December 2013 are shown for CCD A. Systematic position differences on the  $\pm 10$  mas level are seen. Plots for the other CCDs look almost identical. Remaining systematic errors in UCAC4 alone can explain these differences (Zacharias et al. 2013) and were expected to show up here due to the poor charge transfer efficiency of the UCAC CCD. No “corrections” to URAT1 as a function of magnitude (over the non-saturated regime) were applied here in order to not propagate such UCAC4 errors into URAT1.

Fig. 8 shows the residuals of the same data set as a function of color. Most systematic differences are within  $\pm 5$  mas. The same type of plots of other data sets look similar. No corrections for differential color refractions (DCR) were applied. From theoretical estimates the effect of DCR on URAT1 position data is found to be below our systematic error floor, which is confirmed by residual plots as function of color. Figs. 7 and 8 were generated after correcting for other systematic errors

as explained next.

#### 4. Systematic error calibration

##### 4.1. Pixel phase error

Small systematic position errors as a function of the sub-pixel location of stellar image centers are seen in the astrometric solution residuals. As expected these follow a sine-curve as a function of pixel phase. The amplitude ( $A$ ) of the sine-curve is related to  $w$ , the full width at half maximum (FWHM) of the image profile, by an exponential function:

$$A = a e^{-bw}$$

The parameters  $a$  and  $b$  were determined from a linear least-squares fit to sample data, separately for each CCD and coordinate. For the smallest observed image profile width in URAT data, about 1.8 pixel FWHM, the maximal amplitude is about 20 mas. For typical data the amplitude is about 10 mas and quickly drops off to insignificant levels at  $\text{FWHM} \geq 2.5$  pixel.

Individual position corrections to URAT1 observations are then applied for each image and coordinate based on the sine-function of pixel phase value and amplitude as derived for a given exposure's mean FWHM (from quality control data). Resulting residuals showed a small remaining effect which was corrected by updating the parameters for the pixel phase errors.

##### 4.2. Field distortion pattern

Residuals of astrometric solutions using UCAC4 reference stars were stacked up as a function of  $x, y$  coordinate in the focal plane, separately for each CCD. Fig. 9 shows an example of such a field distortion pattern (FDP) for CCD C based on residuals of 140 exposures of acceptable quality of a night in March 2014. The position difference vectors were scaled by a factor of 5000. The FDPs of the 4 CCDs look different due to the combination of optical distortion (lens and dewar window) and individual tilt with respect to the ideal focal plane. However, the level of systematic errors is very similar as given in Table 2.

Sample FDPs of data of the same night but split by magnitude, or color of stars, or by exposure time were identical within the random noise level

of about 3 to 5 mas RMS. Comparing data from different nights, or split by declination or early part versus later part of a night displayed typical RMS differences of about 5 to 10 mas with somewhat correlated vectors over the field of view. This result is not fully understood but changing temperature gradients across the CCDs are suspected to play a role.

The FDPs of several nights were averaged to a mean FDP which was applied to the  $x, y$  data. After application of the mean FDP the residual FDP pattern was much smaller but seemed to still show some systematics. The process was iterated once to arrive at a single final FDP (per CCD) which was used for calibrating all URAT1 data.

##### 4.3. General magnitude equations

Flip observations (section 2.7) provide pairs of observations of the same area in the sky and the same CCD with  $x, y$  data in 2 orientations rotated by  $180^\circ$  between the data sets. Mapping between 2 such exposures was performed using a full 2nd order polynomial model (12 parameters) with over 1000 stars in a weighted least-squares adjustment. Residuals were then binned and plotted as a function of magnitude.

Fig. 10 shows an example for CCD B and exposure pair 7999 versus 8015 (60 sec). Larger than average scatter is seen at the very bright end (due to few stars) and the faint end (due to large  $x, y$  center errors). Note that traditional saturation is at about 6.5 mag on this scale. For stars brighter than that, the CAB feature allows for useful astrometric data.

If there were a pure magnitude equation (systematic position shift as function of magnitude) caused by the instrument (lens plus camera and readout) those systematic errors would show up with doubled amplitude in these flip observations. A coma-like magnitude equation (systematic position shift as a function of the product of magnitude and  $x, y$  coordinate) would show up in the same way. For UCAC data, for example, the coma-like systematic errors are in the order of  $\pm 100$  milli-pixel (mpx) over 6 magnitudes caused by a poor charge transfer efficiency of that CCD. With URAT1 data we see here nothing of significance with an upper limit of about  $10 \text{ mpx} / 2 = 5 \text{ mpx}$ .

There is a degeneracy between a pure magni-

tude equation and a coma-like term as seen in these flip observations. If they are of exactly the same amplitude with opposite sign they would cancel out and show a flat result like seen in Fig. 9, however, that is very unlikely.

Plots for the other CCDs and other pairs of flip observations look very similar. There are no indication of a significant magnitude equation or coma-like term in URAT1  $x, y$  data.

#### 4.4. Grating images

Differences between  $x, y$  positions of central images and first order images of grating observations were calculated. Data from the same exposure were analyzed which give only a small magnitude range with both 0th and 1st order images having sufficient signal-to-noise (S/N) as well as not being saturated. Similarly  $x, y$  transformations were performed between the 0th order data of 30 sec exposures and 240 sec exposures of 1st order data to extend the range of overlapping magnitudes. In all investigations no systematic difference between the positions of 0th and 1st order images were found.

#### 4.5. Astrometric calibration near saturation

Although the CAB feature of our CCDs allows us to acquire positions of stars from successful  $x, y$  center fits up to about 2.5 magnitudes brighter than saturation, those data are subject to systematic errors as compared to unsaturated data. Regular survey observing provides a short (60 sec) and a long (240 sec) exposure of each observed field. Thus the long exposure saturates at about 1.5 mag earlier than the short exposure.

Using only stars of instrumental magnitude 12 or brighter, the  $x, y$  data of a long exposure is matched with the data of the short exposure using a linear transformation model. The residuals as a function of magnitude, separately for each CCD and coordinate, reveal the desired systematic position offset of saturated data with respect to unsaturated data. An example is given in Fig. 11 for a single night and CCD A. Data for other CCDs look similar. Here the instrumental saturation magnitude is near 6.8. In the range of 6.8 to 5.3 mag the short exposure is still unsaturated and is assumed to be “error free”. The position difference seen

in that range thus shows the systematic error of the long exposure beyond the traditional saturation. For instrumental magnitudes brighter than 5.3 mag the short exposure also becomes saturated and begins to show the same relative offset (with respect to error free) as the long exposure. Assuming the (observed long exposure – true) position difference continues on a linear function with magnitude for stars brighter than (saturation mag - 1.5 mag), we would expect to see a constant position difference in these plots for stars brighter than about 5.3 mag. That is what we see for the  $x$ -coordinate in our example.

For the  $y$ -coordinate in Fig. 11 we see a drop in the observed position differences for stars brighter than about instrumental magnitude 5.3 indicating an actual deviation from the simple linear position correction model. Empirical corrections were derived based on 2 linear stretches in the overexposed magnitude regime with corresponding free parameters for the magnitudes at which each linear stretch begins and ends (i.e. 3 magnitudes and 2 slope parameters total).

Data from different nights were analyzed showing a break in the pattern, some of which correspond to changes in the camera electronics (swap or replacement of boards which control the read-out of the main camera CCDs). Some data show position offsets exceeding 100 mas at about 2 magnitudes brighter than traditional saturation, others show total errors of only about 10 mas. A total of 6 groups as function of epoch could be identified. Separate systematic position error corrections for the overexposure regime were derived for the data in each of the groups and for each CCD and coordinate. The corrections were then checked against the observed residuals of astrometric solutions using UCAC4 reference stars. Remaining systematic errors are expected to be  $\leq 10$  mas up to about 1.5 magnitudes brighter than traditional saturation and somewhat larger for even brighter stars.

## 5. The Catalog

Some basic numbers of the URAT1 catalog are given in Table 3. The URAT1 data are provided by binary zone files each covering 0.2 deg along declination. Each entry has 80 bytes of integer data which is explained in Table 4. Sample files in ASCII, a detailed “readme” file, in-



dex files and basic access code are provided with the public release. URAT1 is not distributed by USNO, instead is kindly served by CDS, Strasbourg through Vizier as catalog I/329. The distribution of URAT1 stars by magnitude is shown in Fig. 12.

### 5.1. Mean positions

Weighted mean positions were obtained separately for each of the 38 data sets (see above) from the astrometric solutions after having applied systematic error corrections for pixel phase error, field distortions, and for stars in the CAB regime. These positions were then combined to a weighted overall mean position given in the URAT1 catalog. Thus URAT1 is an observational catalog providing positions on the International Celestial Reference Frame (ICRF) via UCAC4 reference stars which are believed to be on the Hipparcos system. The mean epoch of stars in URAT1 is slightly different for each star within the range of 2012.3 to 2014.7. Most stars have a mean epoch closer to the center of that range but some objects were observed only early or late within this range (sky coverage, limiting magnitude).

To make it into the catalog a star needs to have at least 3 observations or a match with the 2MASS point source catalog within 3 arcsec. The average number of observations per star is 24. The distribution of URAT1 position errors (from scatter of individual observations) is shown in Fig. 13.

### 5.2. Proper motions

Preliminary proper motions were calculated exclusively from combining the observed, mean URAT1 positions with 2MASS positions at about 15 years earlier. Typical proper motion errors are about 5 to 7 mas/yr (see Fig. 14). The proper motion errors given in the URAT1 catalog are formal errors based on the individual epoch difference and positional errors of the 2 catalogs involved, assuming a constant 80 mas error for 2MASS data independent of brightness. Note, stars with few observations (like 1 or 2) and large proper motions in URAT1 need to be taken with caution, particularly in crowded areas, because of possible accidental (wrong) matches with 2MASS entries.

### 5.3. Added data

URAT1 observational data are supplemented by 2MASS J,H, and  $K_s$  magnitudes and some 2MASS flags for about 83% of stars in common. The AAVSO Photometric All Sky Survey (APASS) provided B,V,g,r,i magnitudes for about 16% of the URAT1 stars. The APASS photometry is taken from DR8 plus single observations not yet published elsewhere.

### 5.4. Contamination and completeness

Possible reasons for false entries in URAT1 include issues with close doubles/blended images, minor planets, CCD defects, artifacts near bright stars, and contamination from the grating image assignment process. An upper limit of the number of false objects in URAT1 is estimated by the list of 1.1 million objects not found in GSC 2.4 (see below), which is less than 0.5% of the URAT1 catalog entries.

URAT1 is not complete, even in the areas covered by observations. Blended images, close double stars, and any “problem” case during the reductions were just dropped. The goal here is to provide the user with an accurate, dense reference star catalog at current epochs.

## 6. External Comparisons

The URAT1 catalog as of November 2014 was extensively validated in-house and by selected external reviewers. Results for positions and proper motions are summarized in Table 5.

### 6.1. Primary systems

At the bright end URAT1 was compared directly to the Hipparcos Catalog (van Leeuwen 2007). No significant mean position differences (within about 5 mas) were found, confirming the URAT1 catalog to be on the Hipparcos / ICRF system. Observed URAT1 positions of over 66,000 stars in common with the Hipparcos Catalog were compared at the URAT1 mean observational epoch using the Hipparcos Catalog positions and proper motions. For more details see (Zacharias 2015).

At the faint end URAT1 provided observations of 958 ICRF2 (Fey et al. 2009) counterparts. Excluding outliers, mean URAT1 positions of the remaining 849 sources are consistent with the ICRF

within about 10 mas (see Fig. 15). This is the single, largest systematic error seen with URAT1 so far and a more detailed investigation including more extragalactic radio sources is under way. However, these data indicate an upper limit of a possible magnitude dependent systematic error in URAT1 over its large range of over 12 magnitudes (Hipparcos stars to faint end ICRF sources) of about 10 mas for Dec and less than that for RA.

URAT1 proper motions of the ICRF sources are around zero as expected (Fig. 16). Similarly over 14,000 extragalactic sources of the second Large Quasar Astrometric Catalog (LQAC2) (Souhay et al. 2012) are found in URAT1. Their observed mean proper motions as function of declination zone and magnitude are typically within  $\pm 0.5$  mas/yr and up to about 2 mas/yr for some samples. A position comparison of these sources is not meaningful because of the relative low quality of LQAC2 positions as compared to URAT1.

## 6.2. Deep catalogs

For the comparison with the PPMXL catalog, 2 zones around RA =  $90^\circ$  (z1) and  $300^\circ$  (z2) going over all declinations and covering the 10 to 19 magnitude range were selected. Comparing PPMXL with ICRF2 large systematic differences up to about 40 mas are seen, suggesting that some of the observed URAT1–PPMXL differences are caused by errors in the PPMXL.

An extensive comparison to the Sloan Digital Sky Survey (SDSS) data (Munn et al. 2004) was performed. Positions are compared at the URAT1 observational epoch by using USNO-B proper motions to update SDSS positions. Overall the systematic differences in proper motions are about 0.4 and 0.9 mas/yr for RA and Dec, respectively, with variations as a function of field on the sky with a standard deviation of 1.8 mas/yr. The differences in positions are correlated with the proper motion differences and a small magnitude equation is seen in each coordinate (about  $\pm 8$  mas between magnitude 14 and 19).

A match of the URAT1 stars with GSC 2.4 was performed (R. Smart, private com. 2014). A total of 1.1 million URAT1 entries are not found in the GSC data, which is believed to be very “clean” and complete. A spot check of about 30 of those objects (random selection) versus the real sky re-

veals a mix of different cases. Some objects are clearly seen on the digital sky images, some are in crowded fields, others point to very faint objects, no object at all or close to an object, indicating a possible large proper motion. Thus not all but an unknown fraction of these 1.1 million objects could be artifacts, or images of moving objects in URAT1. This result sets a limit of the contamination level in URAT1. Likely over 99.5% of URAT1 objects are real, stellar or extragalactic sources.

## 6.3. PM2000

A detailed comparison of URAT1 data with the PM2000 catalog (Ducourant et al. 2006) was performed (C. Ducourant & R. Teixeira, private com. 2015). The PM2000 catalog covers the Bordeaux Zone ( $+11^\circ \leq \delta \leq +18^\circ$ ) of the Astrophysical Catalogue (AC) project from around 1900. The AC plates were reduced with Hipparcos and combined with epoch near 2000 transit circle CCD data to arrive at positions and proper motions for stars in the about 7 to 16 mag range on the ICRF using a global adjustment. Thus these data are completely independent of URAT1 and UCAC4. URAT1 agrees with PM2000 extremely well for RA with systematic position differences  $\leq 5$  mas over the 8 to 16 mag range and as function of RA, with no magnitude equation (Fig. 17). An almost constant position offset of about 10 to 15 mas is seen for Dec, again with no magnitude equation. Large position differences up to 50 mas in Dec are seen between PM2000 and URAT1 at the bright limit magnitude of PM2000 ( $V = 7$ ). This is not seen when comparing URAT1 with Hipparcos directly.

The systematic proper motion differences between URAT1 and PM2000 are between 0 and 1.2 mas/yr. A noticeable increase in the RMS proper motion differences is seen in the galactic plane, which can be explained by confusion of URAT1 to 2MASS matches and thus contaminating the sample with some false proper motions.

## 6.4. Other comparisons

Over 57,000 stars of the Lepine and Shara Proper Motion (LSPM) catalog (Lépine & Shara 2005) are found in URAT1. Due to the respective cut-offs of the catalogs only stars with proper motions in the about 150 to 250 mas/yr range are seen.

Both the LSPM relative and absolute proper motions were compared with URAT1. There is good agreement for RA but not for Dec.

Vector point diagrams were derived from URAT1 data (R. Teixeira, private com. 2015) using 48 near equal area regions on the sphere. Except for the over-density of proper motions around 200 mas/yr (again likely a contamination issue in crowded fields) the main result is that statistical behavior of URAT1 data is consistent with predictions of the Galaxy model (Besancon model). No abnormalities are seen in the spacial distribution of URAT1 proper motions.

Minor planet occultation predictions were analyzed (D. Harald, private com. 2014). Compared with previously used UCAC4 data a noticeable improvement for the sample of 90 events observed in the past is seen when using URAT1 data. This check on many random fields indicates good astrometric performance of URAT1 data for applications which are sensitive on the 10 mas level of accuracy.

## 7. Discussion and Conclusions

The distribution of URAT1 proper motions on the sky shows the effects of solar motion and galactic rotation and thus gives some confidence in the overall accuracy of URAT1 astrometry (no significant spacial biases). Systematic differences of proper motions between URAT1 and several other external data are on the 1 to 2 mas/yr level. At this point it is not clear which data set has the smallest systematic errors.

The systematic position error floor of URAT1 data is likely around 10 mas. URAT1 data match the current celestial reference frame at the bright end (Hipparcos Catalog) and the faint end (ICRF counterparts) very well, which suggests insignificantly small magnitude equations in URAT1 data. Local, spacial systematic errors of URAT1 positions and proper motions have not been investigated in detail. However, such errors are not to be expected due to the “averaging” URAT observing method (same star imaged on different CCDs and different parts of a CCD) and the homogeneous astrometry of 2MASS.

URAT1 has a very low level of contamination by false entries (few tenth of a percent at most) as seen from comparisons with the GSC and other

data. Possibly some minor planets have made it into the catalog. Other false objects will include artifacts near bright stars or detections associated with blended images. Some proper motions in URAT1 will be wrong due to mis-matches with 2MASS, particularly in dense fields. URAT1 is not intended to be complete but should be complete to over 90% in the sky area covered and 3 to 18 mag range due to the observing and reduction methods used.

URAT1 can serve as accurate reference star catalog before Gaia data become available. The position accuracy of URAT1 is about 4 times higher than for UCAC4 data at its faint end and the sky density of URAT1 is about 4 times larger than that of UCAC4, similar to the sky density of 2MASS.

The USNO management is thanked for supporting this project: K.J.Johnston, B.Luzum (the former and current scientific directors of USNO), R.Gaume, B.Dorland (the former and current head of the astrometry department), and P.Shankland (the director of NOFS). Semiconductor Technology Associates (headed by R. Bredthauer) provided continued support for the URAT camera and dewar long after delivery. The American Association of Variable Star Observers (AAVSO) is thanked for providing unpublished APASS data for our project. 2MASS was used for near IR photometry and as first epoch of URAT1 proper motions. Bill Gray (Project Pluto) is thanked for making available a C code version of our URAT1 access software: [www.projectpluto.com/urat.htm](http://www.projectpluto.com/urat.htm) Aladin and Vizier were invaluable tools provided through CDS, Strasbourg. CDS Strasbourg is also thanked for hosting the URAT1 catalog. DS9 by the Smithsonian Astrophysical Observatory was used as display tool for FITS pixel data files. NOAO is thanked for IRAF, which was used for image analysis while troubleshooting and performing spot checks. Pgplot by California Institute of Technology was used to produce plots.

## REFERENCES

- Ducourant, C., Le Campion, J.F., Rapaport, M., et al. 2006, *A&A*, 448, 1235
- Fey, A., Gordon, D., & Jacobs, C.S. (Eds.), *IERS Tech.Note 35*, Frankfurt, 2009

- Laux, U., & Zacharias, N. 2005, in Proc. APS conf.ser. 338, "Astrometry in the Age of the Next Generation of Large Telescopes", Eds.: K.Seidemann & A.K.B.Monet, p.184
- Lépine, S., & Shara, M. M. 2005, AJ, 129, 1483
- Munn, J., Monet, D.G., Levine, S.E., et al. 2004, AJ 127, 3034
- Souchay, J., Andrei, A. H., Barache, C. et al. 2012, *Å*, 537, 99
- Skrutskie, M.F, Cutri, R.M., Stiening, R., et al. 2006, AJ, 131, 1163
- van Leeuwen, F. 2007, Springer Science Library, Vol. 350
- Vukobratovich, D., Valente, T., Shannon, R.R., Hooker, R., & Sumner, R.E. 1992, "Design and construction of an astrometric astrograph", in proc. "Current Developments in Optical Design and Optical Engineering II", SPIE proceedings Vol. 1752 (doi:10.1117/12.130737), Eds. Robert E. Fischer & Warren J. Smith
- Zacharias, N. 2002, in Proc. SPIE 4836, Eds. T.A. Tyson & S. Wolff, p.279
- Zacharias, N. 2004 in Proc. 3rd Potsdam Thinkshop on robotic telescopes, AN 325, 631
- Zacharias, N., Laux, U., Rakich, A. & Epps, H. 2006, in Proc. SPIE 6267E..227 (astro-ph/0606193v1)
- Zacharias, N., Finch, C.T., Girard, T.M., Henden, A., Bartlett, J.L., Monet, D.G., Zacharias, M.I. 2013, AJ145, 44
- Zacharias, N. 2015, in Proc. ADeLA 2014 meeting (in press), see also arXiv:1506.05853 .

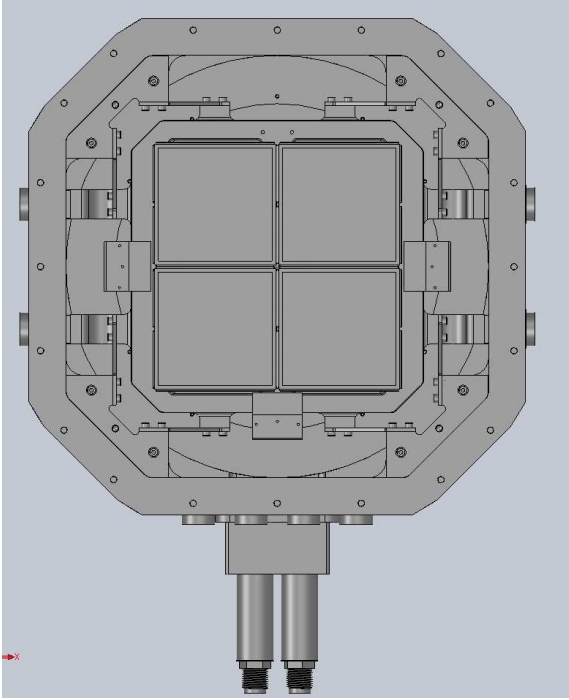


Fig. 1.— Layout of URAT focal plane. Each of the 4 big CCDs is 95 by 95 mm in size. There are 3 more CCDs (right, left, bottom) for guiding and focus determination.

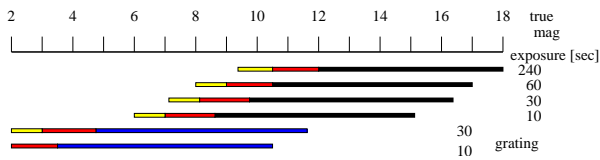


Fig. 2.— Dynamic range of various exposure times and modes of URAT data. Different shades in color represent from right to left: unsaturated regime (black and blue), saturated with CAB allowing good astrometric results (red), and saturated regime with lower quality astrometric calibration (yellow).

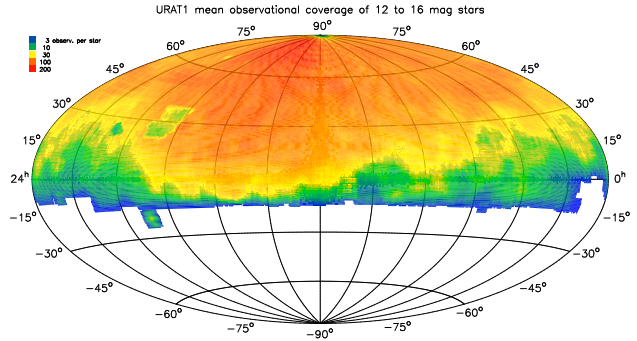


Fig. 3.— Sky coverage of URAT1 catalog data. Color coding indicates the average number of observations per star for stars between magnitude 12 and 16.

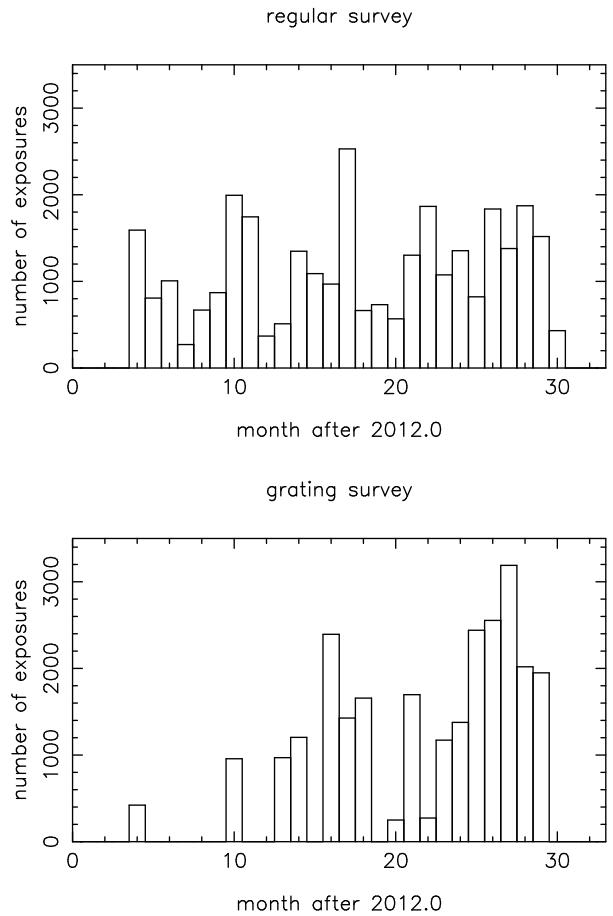


Fig. 4.— Number of exposures used for URAT1 by month after 2012.0 (4 is April 2012, 13 is January 2013). Data for the regular and grating survey are shown separately.

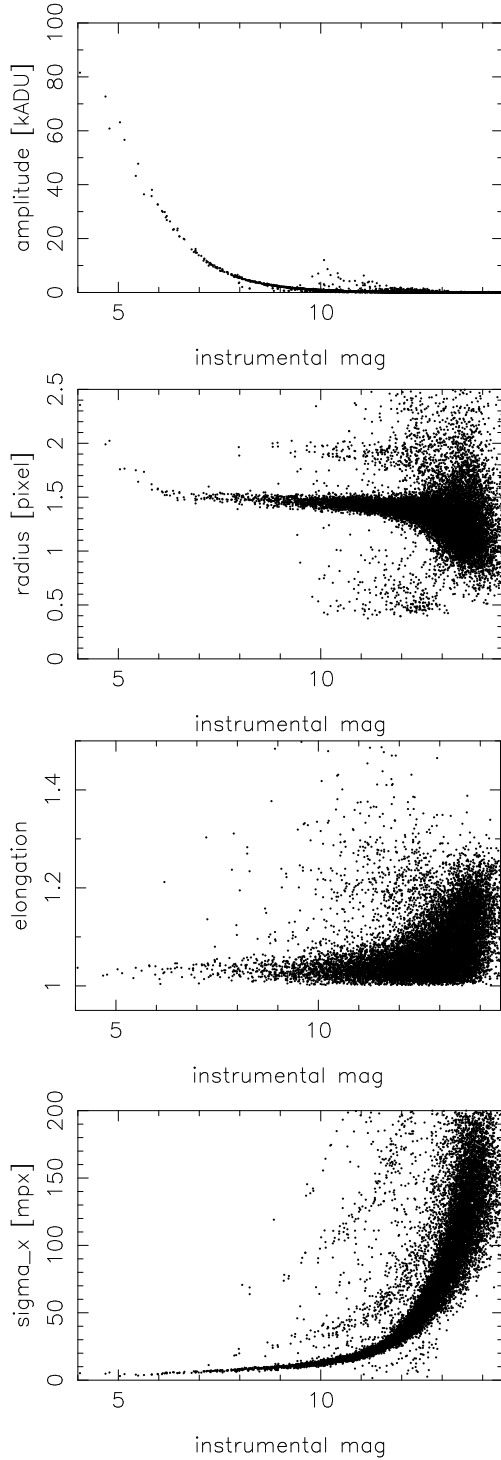


Fig. 5.— Individual stellar image profile fit results as a function of instrumental magnitude; from top to bottom: amplitude, radius, elongation, and center error per coordinate. Results for exposure 14064 (10 sec) of CCD B are shown.

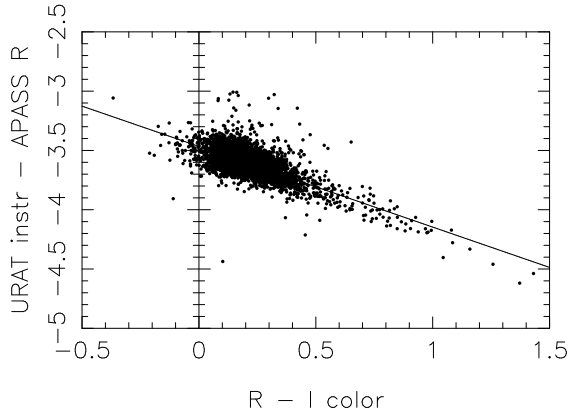


Fig. 6.— Example of color-color data correlation used to determine photometric constant between URAT instrumental and calibrated magnitudes per exposure and CCD using APASS R and I data.

Table 1: Basic data of the telescope, camera, and survey exposures used for URAT1.

telescope	astrograph		
	aperture	203	mm
	focal length	2060	mm
	bandpass	680-762	nm
camera	4 CCDs, each	10.5k x 10.5k	px
	pixel size	9.0	$\mu\text{m}$
	scale	0.905	"/px
	size, each	95 x 95	mm
	field of view	28	sq. deg
guiding	3 CCDs, each	2k x 4k	pixels
	scale	0.80	"/px
regular	2 expos./field	60 & 240	sec
grating	2 expos./field	10 & 30	sec

Table 2: RMS systematic position offsets (millipixel) as a function of location in the focal plane (field distortion pattern).

coordinate	CCD A	CCD B	CCD C	CCD D
	[mpx]	[mpx]	[mpx]	[mpx]
x	22	24	20	15
y	22	26	22	22

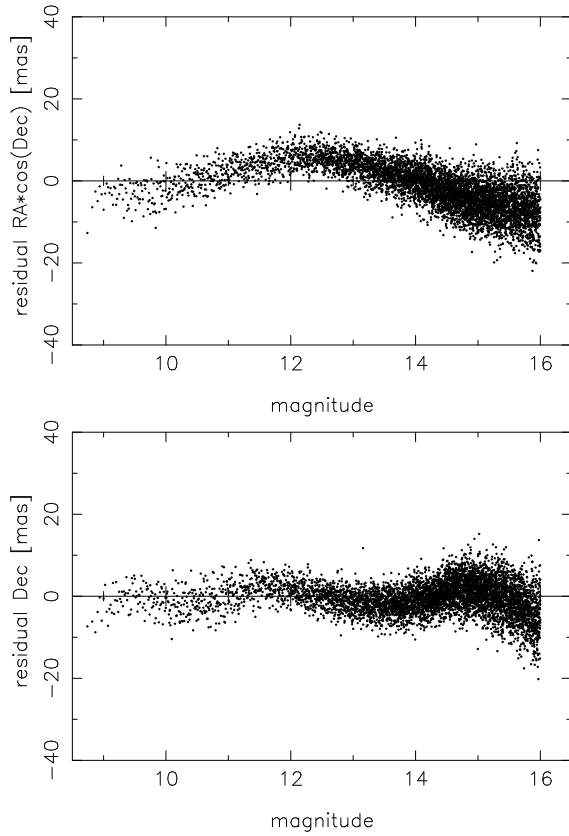


Fig. 7.— Example of residuals (URAT1–UCAC4) for all grating observations in set 13 (Julian date nights 6640 to 6644) of CCD A. Position differences (RA top, Dec bottom) are shown as a function of UCAC4 magnitude. Each dot is the mean over 1000 observations.

Table 3: Characteristics of the URAT1 catalog.

total numb. URAT1 stars =	228276482	
number stars with 1 obs =	10309229	
number stars with 2 obs =	8875122	
average numb. obs/star =	24.3	
number valid 2MASS data =	188656145	82.64%
no 2MASS match stars =	39620337	of
stars >=3 obs., no 2MASS=	39079551	URAT1
number valid APASS data =	37010348	16.21%
APASS stars valid B mag =	29313850	of
APASS stars valid V mag =	30057593	URAT1
APASS stars valid g mag =	32340624	stars
APASS stars valid r mag =	32474206	
APASS stars valid i mag =	28052917	

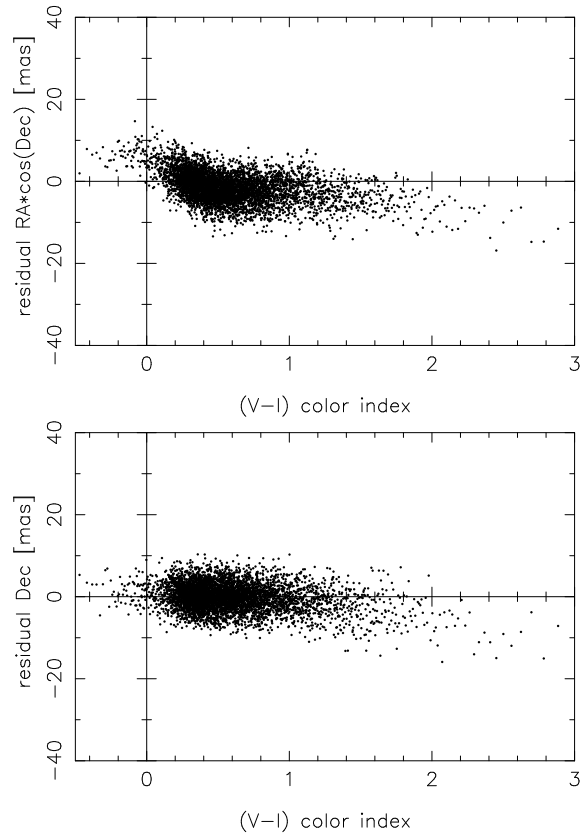


Fig. 8.— Same as previous figure for residuals as a function of V–I color index (from APASS data).

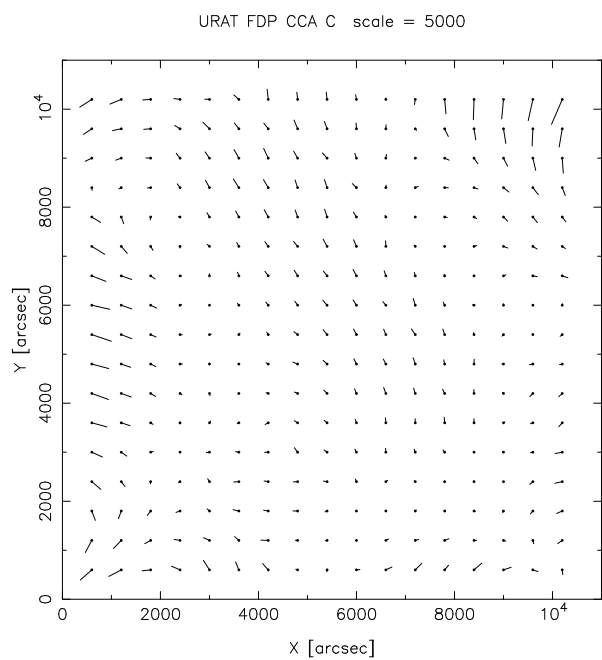


Fig. 9.— Mean field distortion pattern of CCD C as derived from residuals of a single night. The longest vector is about 80 mas.

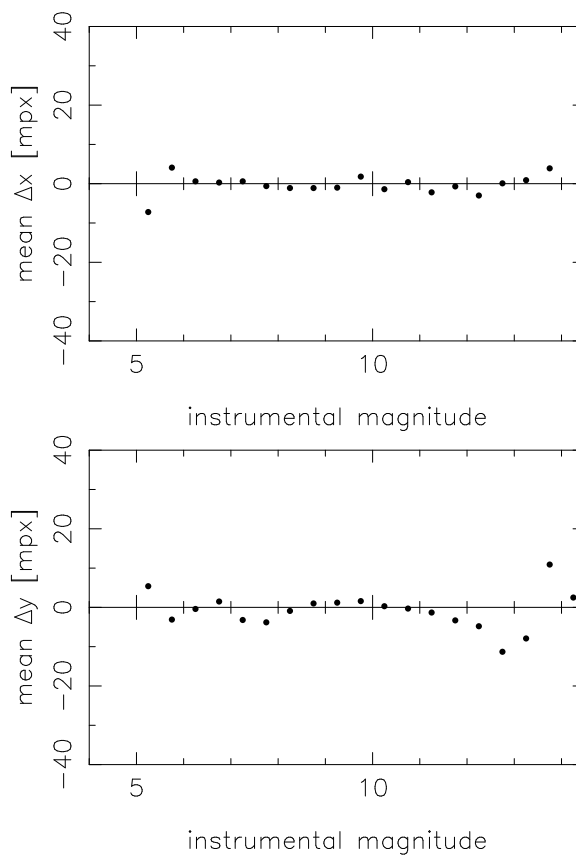


Fig. 10.— Position differences of a flip observation (pair of exposures, regular and  $180^\circ$  rotated with respect to sky) as a function of magnitude.



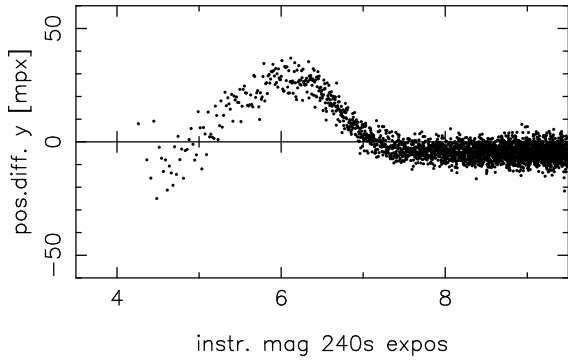
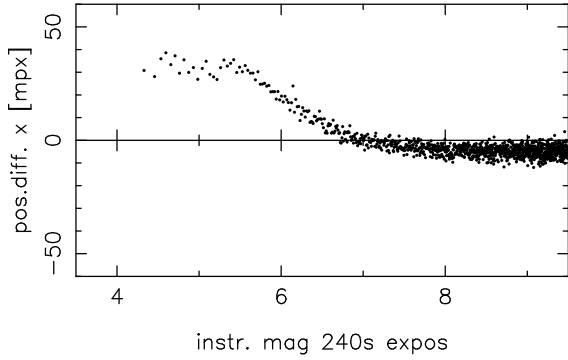


Fig. 11.— Position differences ( $x$  top,  $y$  bottom) between data from long (240 sec) and short (60 sec) regular survey exposures of the same fields. Results for a single night (JD 6828) are shown for CCD A. Each dot represents the mean over 250 stars. Saturation of the long and short exposure begins at magnitude 6.8 and 5.3, respectively, on this scale. Systematic position offsets within this range can be attributed to errors caused by saturation of the long exposure only.

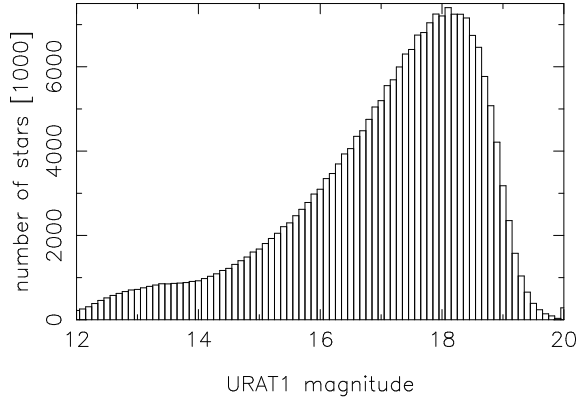


Fig. 12.— Distribution of URAT1 stars by magnitude.

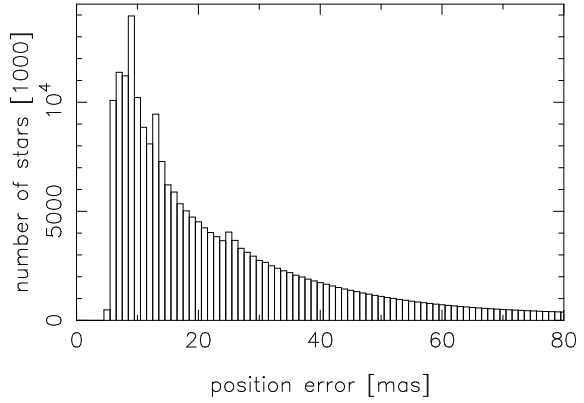


Fig. 13.— Distribution of URAT1 position errors.

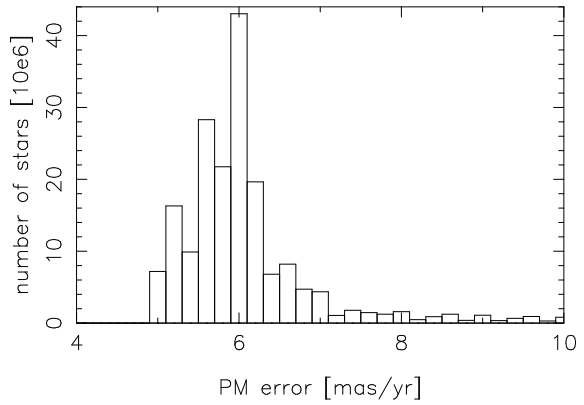


Fig. 14.— Distribution of URAT1 proper motion errors.

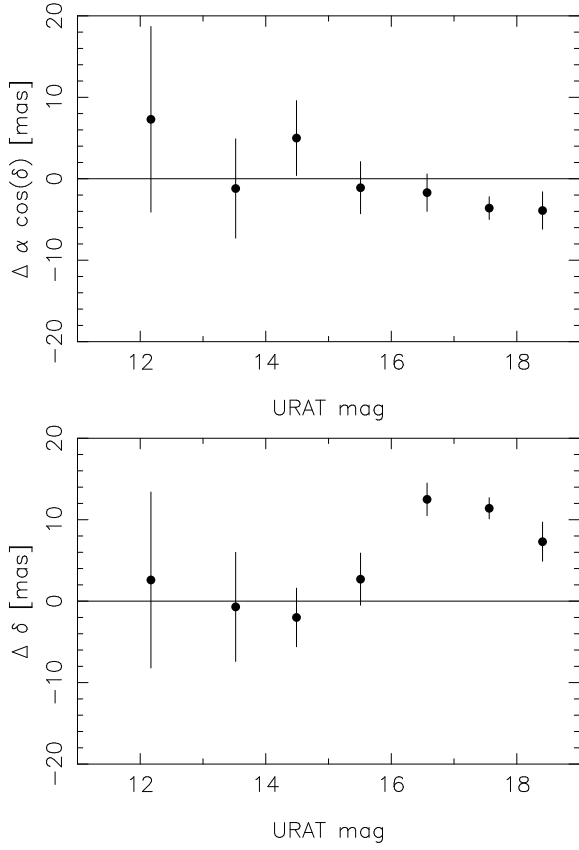


Fig. 15.— Weighted mean position differences URAT1–ICRF2 of optical counterparts directly observed with the astrograph.

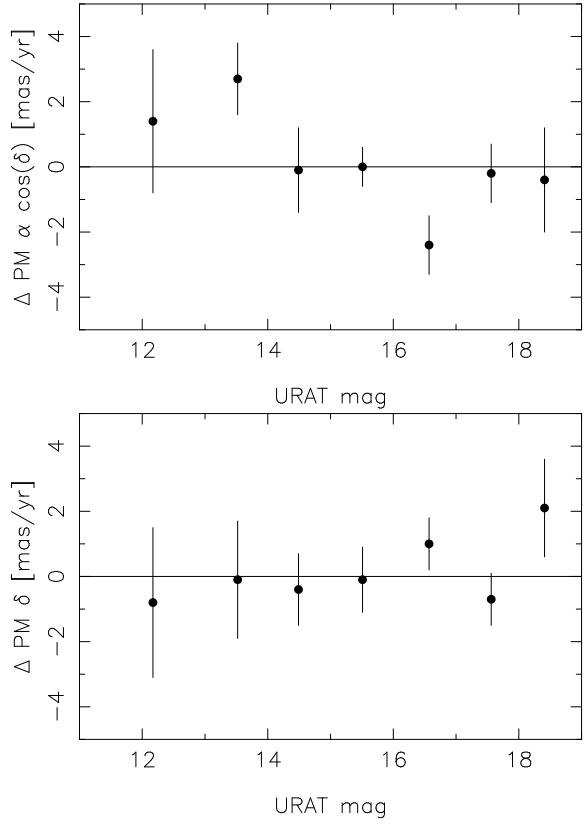


Fig. 16.— Mean URAT1 proper motions of the same ICRF2 counterparts as used for the previous figure.

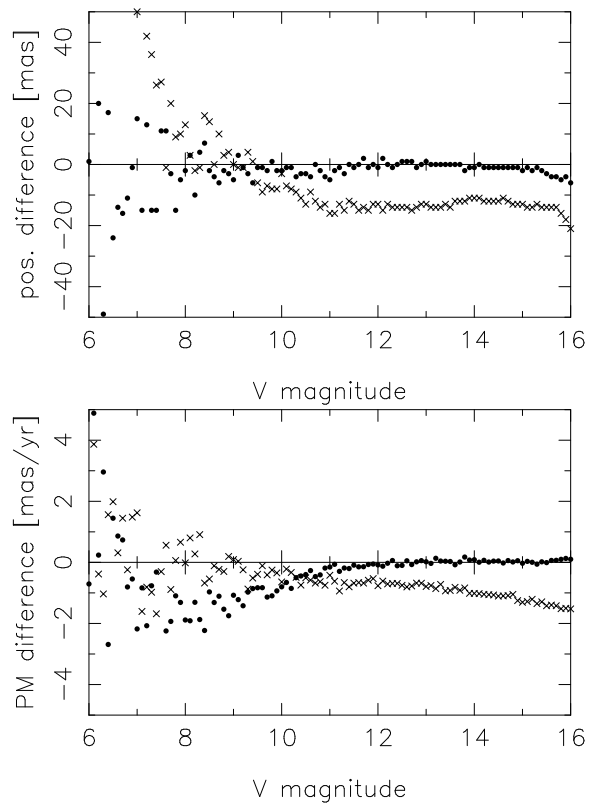


Fig. 17.— Mean PM2000–URAT1 position (top) and proper motion (bottom) differences as a function of V magnitude. Differences for RA are shown with filled circles, while the crosses represent the differences for the Dec coordinate.

Table 4: Description of data items contained in the URAT1 catalog.

col	item	type	unit	description
1	ra	I*4	mas	mean RA on ICRF at URAT1 obs.epoch
2	spd	I*4	mas	mean South Pole Distance
3	sig	I*2	mas	position error per coord.(scatter)
4	sigm	I*2	mas	position error per coord.(model)
5	nst	I*1	--	tot. number of sets star is in
6	nsu	I*1	--	n. of sets used for mean position
7	epoc	I*2	myr	mean URAT1 obs. epoch - 2000.0
8	mmag	I*2	mmag	mean URAT1 model fit magnitude
9	sigp	I*2	mmag	URAT1 photometry error
10	nsm	I*1	--	n.of sets used for URAT1 magnitude
11	ref	I*1	--	largest reference star flag
12	nit	I*2	--	total number images (observations)
13	niu	I*2	--	n.of images used for mean position
14	ngt	I*1	--	total n. of 1st order grating obs.
15	ngu	I*1	--	n. of 1st order grating obs. used
16	pmr	I*2	0.1mas/yr	proper motion RA*cosDec
17	pmd	I*2	0.1mas/yr	proper motion Dec
18	pme	I*2	0.1mas/yr	proper motion error per coord.
19	mf2	I*1	--	match flag URAT1 with 2MASS
20	mfa	I*1	--	match flag URAT1 with APASS
21	id2	I*4	--	2MASS star identification number
22	jm	I*2	mmag	2MASS J mag
23	hm	I*2	mmag	2MASS H mag
24	km	I*2	mmag	2MASS K mag
25	ejm	I*2	mmag	error 2MASS J mag
26	ehm	I*2	mmag	error 2MASS H mag
27	ekm	I*2	mmag	error 2MASS K mag
28	iccj	I*1	--	CC flag 2MASS J
29	icch	I*1	--	CC flag 2MASS H
30	icck	I*1	--	CC flag 2MASS K
31	phqj	I*1	--	photometry quality flag 2MASS J
32	phqh	I*1	--	photometry quality flag 2MASS H
33	phqk	I*1	--	photometry quality flag 2MASS K
34	abm	I*2	mmag	APASS B mag
35	avm	I*2	mmag	APASS V mag
36	agm	I*2	mmag	APASS g mag
37	arm	I*2	mmag	APASS r mag
38	aim	I*2	mmag	APASS i mag
39	ebm	I*2	mmag	error APASS B mag
40	evm	I*2	mmag	error APASS V mag
41	egm	I*2	mmag	error APASS g mag
42	erm	I*2	mmag	error APASS r mag
43	eim	I*2	mmag	error APASS i mag
44	ann	I*1	--	APASS numb. of nights
45	ano	I*1	--	APASS numb. of observ.

Table 5: Summary of external comparisons of URAT1 catalog data. Numbers in parentheses indicate the URAT1 magnitude.

positions:

catalog	dRAcos(D) [mas]		dDec [mas]	
	bright	faint	bright	faint
ICRF2	+6 (12)	-4 (19)	+3..-2..+12..+7	
Hip.2	0 ( 8)		+5 ( 8)	
PPMXLz1	0 ..+5.. 0 ..+20		0 ..-10..-10..-20	
PPMXLz2	+5..+10..+5 ..+15		+10..-10..-25..-10	
SDSS	+9 (14)	-8 (19)	-6 (14)	+8 (19)
PM2000	+2 ( 9)	0 (15)	+10 (10)	+12 (15)

proper motions:

catalog	dRAcos(D) [mas/yr]		dDec [mas/yr]	
	bright	faint	bright	faint
ICRF2	+2.0 .. -2.0 .. 0.0		-0.5 (12)	+0.5 (18)
LQAC2	+2.2 (12)	-0.2 (19)	-0.5 (14)	0.0 (19)
LSPMa	0.0 ( 8)	-0.5 (18)	+1.0 ( 8)	+4.0 (18)
LSPMr	-2.0 ( 8)	-2.0 (18)	-7.0 ( 8)	-3.0 (18)
PPMXLz1	0.0..+0.5..-1.0		-0.8.. 0.0..+1.0	
PPMXLz2	+0.5..+1.0..-0.5		0.0..-0.8..+1.0	
SDSS	+1.0 (14)	-0.1 (19)	-1.7 (14)	-0.2 (19)
PM2000	+1.0 ( 9)	0.0 (16)	0.0 ( 9)	+1.2 (15)